AMERICAN SOCIETY FOR MICROBIOLOGY | Molecular and Cellular Biology

SIK2 Restricts Autophagic Flux To Support Triple-Negative Breast Cancer Survival

Kimberly E. Maxfield,[a,b]* Jennifer Macion,[b] Hariprasad Vankayalapati,[c] Angelique W. Whitehurst[b]

Department of Pharmacology, University of North Carolina at Chapel Hill, Chapel Hill, North Carolina, USA[a]; Simmons Comprehensive Cancer Center, UT-Southwestern Medical Center, Dallas, Texas, USA[b]; Early Discovery & Medicinal Chemistry, Arrien Pharmaceuticals, Salt Lake City, Utah, USA[c]

Triple-negative breast cancer (TNBC) is a highly heterogeneous disease with multiple, distinct molecular subtypes that exhibit unique transcriptional programs and clinical progression trajectories. Despite knowledge of the molecular heterogeneity of the disease, most patients are limited to generic, indiscriminate treatment options: cytotoxic chemotherapy, surgery, and radiation. To identify new intervention targets in TNBC, we used large-scale, loss-of-function screening to identify molecular vulnerabilities among different oncogenomic backgrounds. This strategy returned salt inducible kinase 2 (SIK2) as essential for TNBC survival. Genetic or pharmacological inhibition of SIK2 leads to increased autophagic flux in both normal-immortalized and tumor-derived cell lines. However, this activity causes cell death selectively in breast cancer cells and is biased toward the claudin-low subtype. Depletion of ATG5, which is essential for autophagic vesicle formation, rescued the loss of viability following SIK2 inhibition. Importantly, we find that SIK2 is essential for TNBC tumor growth *in vivo*. Taken together, these findings indicate that claudin-low tumor cells rely on SIK2 to restrain maladaptive autophagic activation. Inhibition of SIK2 therefore presents itself as an intervention opportunity to reactivate this tumor suppressor mechanism.

Breast cancer is an extremely heterogeneous disease that is classified by the presence of estrogen receptor (ER), progesterone receptor (PR), and human epidermal growth factor receptor 2 (HER2). Cases where <1% of cells express ER, PR, or HER2 are considered triple-negative breast cancer (TNBC) (1). These molecular markers can serve as a critical stratification tool for tailoring effective therapies to sensitive patients. For example, antiestrogens such as tamoxifen are highly effective in ER-positive patients, and HER2-positive tumors are responsive to trastuzumab (2, 3). Conversely, TNBC tumors lack these targetable proteins, limiting first-line treatment to a combination of radiation and chemotherapy. This approach has changed little over the last 20 years and is characterized by high toxicity and frequent relapse of chemorefractory disease (4). Furthermore, levels of overall and disease-free survival in TNBC are significantly worse than those of other subgroups of breast cancer (5). Thus, for TNBC there is a dire need for less toxic therapies that target the major fulcrums supporting tumor cell survival.

In addition to clinical and pathological markers, extensive gene expression profiling efforts by a number of groups have identified multiple intrinsic molecular subtypes within breast cancer. These subtypes include luminal A and B, which comprise the majority of ER- and PR-positive cases, as well a HER2-enriched clade. Importantly, this analysis has revealed substantial heterogeneity within TNBC. Broadly, TNBC can be subclassified into 2 intrinsic subtypes, basal like and claudin low, but up to 6 additional subclasses have been identified (6–9). Significantly, these groups can be aligned with sensitivity to specific therapies and overall patient survival (4, 6–8, 10). A number of recent studies have indicated that the spectrum of subtypes found *in vivo* is represented among existing tumor-derived cell lines (8, 9, 11). Thus, these cell lines offer a model system that faithfully recapitulates the heterogeneity of the human disease and could reveal subtype-selective vulnerabilities.

Here, we have applied genome-scale loss-of-function screening in both the claudin-low and basal-like subtypes to discover molecular targets for TNBC. We find that salt-inducible kinase 2 (SIK2) is essential for survival, particularly in the claudin-low subtype. There are 3 salt-inducible kinases (SIK1, SIK2, and SIK3), which are best characterized as regulators of gluconeogenesis. Upon glucagon stimulation, protein kinase A (PKA) inactivates SIK, thereby relieving inhibitory phosphorylation of CRCT2/3, which then cooperates with CREB to activate gluconeogenic transcriptional programs (12, 13). Importantly, tissue-specific deletions of SIK proteins in mice can lead to altered glucose and lipid metabolism (14–16). Additional findings have also implicated SIK2 proteins in modulating autophagy and inflammatory responses (17–21). With respect to cancer, two reports have indicated that SIK2 is essential for centrosome splitting and mitotic progression, and SIK1 loss can inhibit anoikis and promotes metastases (22–24).

The contribution of SIKs to biological processes that are often misregulated in human disease has driven efforts to develop small-molecule inhibitors. SIKs are members of the AMPK family but are unique in this group, as they contain a low-stearic-hindrance residue (threonine) at their gatekeeper site (25, 26). This small residue creates an extended hydrophobic pocket that en-

Received 30 June 2016 **Returned for modification** 23 August 2016
Accepted 23 September 2016

Accepted manuscript posted online 3 October 2016

Citation Maxfield KE, Macion J, Vankayalapati H, Whitehurst AW. 2016. SIK2 restricts autophagic flux to support triple-negative breast cancer survival. Mol Cell Biol 36:3048–3057. doi:10.1128/MCB.00380-16.

Address correspondence to Angelique W. Whitehurst, angelique.whitehurst@utsouthwestern.edu.

* Present address: Kimberly E. Maxfield, Food and Drug Administration, Silver Spring, Maryland, USA.

Supplemental material for this article may be found at http://dx.doi.org/10.1128/MCB.00380-16.

hances flexibility and, thus, autoactivation of the kinase (27, 28). This pocket can also selectively accommodate small-molecule inhibitors that would otherwise be occluded by a bulky side chain. For example, AMPK contains a methionine at this residue, suggesting that SIK inhibitors would have minimal off-target activity.

We find that in TNBC, SIK2 functions to restrict autophagy, which in the claudin-low subtype is essential for viability. The contribution of autophagy to tumorigenesis has been somewhat contentious. Autophagy is reported to function both as a tumor suppressor mechanism as well as a survival mechanism, depending on the tumor cell context (29). With respect to TNBC, a recent study found that a subset of ER-negative tumors exhibit downregulation of the critical autophagic protein and tumor suppressor, beclin-1. These patients exhibited poorer overall survival, suggesting that restriction of autophagy in receptor-negative, advanced disease promotes tumor survival (30). Our findings suggest inhibition of SIK2 could release this brake on autophagy and thus presents a therapeutic strategy in the claudin-low subtype.

MATERIALS AND METHODS

Cell lines. Cell lines were obtained from the ATCC with the following exceptions: SUM159, SUM149, and HuMEC (Charles Perou, University of North Carolina at Chapel Hill [UNC]); HME50-hTERT (Jerry Shay, UT Southwestern [UTSW]); WHIM12 (Matthew Ellis, Baylor College of Medicine); HCC1806, HCC1143, and HCC1395 (Gray Pearson, UTSW); HCC1937, HCC1954, HCC38, U2OS, and U2OS-GFP-LC3 (Michael White, UTSW); 293T, MDA-MB-231, and Hs578t (Gary Johnson, UNC); and MDA-MB-157 and HCC1569 (Ganesh Raj, UTSW). All cell lines were cultured in the provider's recommended medium. Cell lines were authenticated using short tandem repeat analysis (STR).

Antibodies and reagents. The following antibodies were used for immunoblotting: SIK2 (6919; 1:1,000), LC3B (3868; 1:1,000), total ULK1 (8054; 1:1,000), phospho-ULK1 (serine 555) (5869; 1:1,000), p62 (8025; 1:1,000), CRTC2 (3926; 1:1,000), and ATG5 (1:1,000) (all from Cell Signaling Technologies); extracellular signal-related kinase 1/2 (ERK1/2) (sc-93; 1:1,000; Santa Cruz); SIK2 (636702; 1:1,000; BioLegend); phospho-CRTC2 (serine 275) (1:1,000; gift from Olga Goransson, Lund University); phospho-histone 3B (serine 10) (1:200; Millipore); and pericentrin (1:1,000; AbCam). Antibodies used for immunofluorescence were V5 (Life Technologies) and p62 (sc-28359; 1:100; Santa Cruz). The SIK2 inhibitor ARN-3236 was obtained from Arrien Pharmaceuticals, Inc. HG-9-91-01 was obtained from Fisher Scientific. CellTiter-Glo (CTG) was purchased from Promega. Lipofectamine RNAiMAX was purchased from Thermo Fisher Technologies. Opti-MEM and Hoechst 3342, trihydrochloride, trihydrate were obtained from Thermo Fisher Scientific. Paclitaxel was obtained from Tocris Bioscience.

Expression plasmids and mutagenesis. Human SIK2 (clone IOH45349) was obtained in pENTR221 from the Ultimate ORF (open reading frame) collection from Thermo Fisher Technologies (housed at UTSW). pENTR221 SIK2 was cloned into pLX302 using the Gateway cloning system (Thermo Fisher Scientific). Kinase-dead SIK2 (K49M) was generated using site-directed mutagenesis using the following primers: forward, ACCAAGACGGAGGTGGCAATAATGATAATCGATAAGTC TCAGC; reverse, GCTGAGACTTATCGATTATCATTATTGCCACCTC CGTCTTGGT.

Viral packaging plasmids pCMV-dr8.91 and pCMV-VSV-G were a gift from Michael White (UTSW). pCDH-GFP-LC3 (Channing Der, UNC) was used for GFP-LC3 SUM159 cells. For SIK2 short hairpin RNA (shRNA), PLKO.1 SIK2 shRNA clones TRCN0000196955 and TRCN0000037494 and PLKO.1 nonsilencing control (from the Broad Institute RNAi Consortium) were purchased from Sigma.

Cell viability assays. Cells were reverse transfected in 96-well format. One hundred twenty hours postplating, luminescence values were read following addition of 15 μl of Cell Titer-Glo on a PHERAstar Plus (BMG) plate reader. Where indicated, cells were exposed to a final concentration of 1 nM paclitaxel 48 h postplating. For ARN-3236 treatment, cells were plated and simultaneously treated with 2 μM ARN-3236 or vehicle control. Forty-eight hours later, cells were treated again with 2 μM ARN-3236. Viability readings were taken 96 h after plating. For HG-9-91-01 treatment, cells were treated as described above with 1 μM the inhibitor.

siRNA transfections. Short interfering RNA (siRNA) pools were obtained from GE Healthcare (M-004778-03; siGENOME siRNA) or Sigma (SASI_Hs01_00054682, SASI_Hs01_00054683, and SASI_Hs01_00054684; Mission). Control siRNA (siCTRL) used was a nontargeting control (D-001206-14 and D-001210-05; GE Healthcare) or siRNA targeting FNDC3B (MU-017856-00; GE Healthcare), which was innocuous in pangenomic screening. Cells were reverse transfected with 8.6 pmol siRNA for CTG and 4.3 pmol siRNAs for all other assays. A toxic siRNA, UBB (M-013382-01; GE Healthcare), was used to monitor transfection efficiency. CTG values for UBB transfection must result in viability loss of >90% compared to the control transfected cells for inclusion.

Pangenomic siRNA screen and data processing. An siGENOME SMARTpool siRNA library targeting 18,171 genes was purchased from GE Healthcare in 96-well plate format. siRNA pools (4.3 pmol) were transfected into cells using Lipofectamine RNAiMax solution. Forty-eight hours later, cells (SUM159, SUM149, HCC1806, and WHIM12) were treated with either vehicle or 1 nM paclitaxel. Ninety-six hours postplating, cell viability was measured using CellTiter-Glo according to the manufacturer's protocol, modified to use 15 μl per well. Measurements were made with a PHERAstar Plus (BMG) plate reader. Individual values were normalized to the medians of their respective rows. The normalized paclitaxel-treated values were divided by the untreated values to derive a synthetic lethal value. Z-scores, based on the means and standard deviations from each plate, then were calculated for each gene for both direct (no paclitaxel) and synthetic behavior. See Table S1 in the supplemental material for Z-scores and normalized viability scores.

Lentiviral infections. Lentivirus was produced through cotransfection of HEK293T cells with 3 μg of viral expression vector, 3 μg of pCMV-dr8.91 packing vector, and 300 ng of pCMV-VSV-G envelope vector using Fugene according to the manufacturer's protocol. Virus-conditioned medium was harvested, passed through 0.45-μm filters, and then used to infect target cells in the presence of 10 μg/ml Sequa-brene. Following infection, stable populations were selected using appropriate antibiotics. For shSIK2, knockdown was validated 2 days following infection (by quantitative PCR [qPCR] and immunoblotting), and downstream assays were performed without selection.

Colony formation assay. One hundred twenty hours after siRNA transfection, cells deemed viable by trypan blue exclusion assay were replated at limiting dilution in 6-well format. Cells were fed twice weekly until control colonies began to merge. Samples were fixed with 3.7% formaldehyde and stained with Giemsa.

Soft-agar assays. For siSIK2 soft-agar assays, SUM159 cells were reverse transfected with 10 pmol of siRNA. Seventy-two hours posttransfection, cells were resuspended in 0.375% Bacto agar in complete medium, and 2×10^3 viable cells were plated over a layer of solidified 0.7% Bacto agar in a 24-well dish. Cells were fed once weekly for 2 weeks and then stained with Giemsa. For SUM159 shSIK2 soft-agar assays, SUM159 cells stably expressing the indicated shRNAs were resuspended in 0.375% Bacto agar in complete medium, and 2×10^3 cells were plated over a layer of solidified 0.7% Bacto agar in 24-well dishes. Colonies were fed once a week for 2 weeks and then stained with Giemsa. For ARN-3236 soft-agar assays, SUM159 cells were resuspended in 0.375% Bacto agar in complete medium, and 2×10^3 cells were plated over a layer of solidified 0.7% Bacto agar in 24-well dishes. Cells were treated with 1 μM ARN-3236 each day for 9 days. Cells were fed once with 2× serum on the sixth day. The cells were stained with 0.05% crystal violet in 10% ethanol. All soft-agar assays were manually counted using a Leica M7z stereoscope.

Gene expression. Total RNA was isolated using an RNA isolation kit (Sigma) and reverse transcribed using the high-capacity cDNA reverse

transfection kit (Life Technologies) according to the manufacturer's instructions. An Applied Biosystems real-time PCR system and TaqMan real-time PCR gene expression assays were used to measure gene expression for SIK2 (Hs01568566_m1) and RPL27 (Hs03044961_g1). Expression values relative to those of RPL27 were calculated using the comparative threshold cycle (C_T) method.

Immunoblotting. Whole-cell lysates were prepared in 2× Laemmli sample buffer and resolved using SDS-PAGE. Gels were transferred to Immobilon polyvinylidene difluoride (PVDF; Millipore), blocked in Tris-buffered saline containing 0.1% Tween 20 (TBST) and either 5% nonfat dry milk or bovine serum albumin (BSA), and incubated with the indicated primary antibodies overnight. After washes in TBST, appropriate horseradish peroxidase (HRP)-coupled secondary antibodies (Jackson ImmunoResearch) were used for chemiluminescence. ImageJ was used to quantitate band intensity.

Immunofluorescence. Cells plated on glass coverslips were fixed with 3.7% formaldehyde and then permeabilized with 0.5% Triton X-100 for 10 min. Cells were blocked and washed in 1% BSA, 0.1% Tween 20 in 1× phosphate-buffered saline (PBTA). Cells were incubated with primary antibodies for 1 h, followed by three washes in PBTA. Coverslips were then incubated with Alexa Fluor-conjugated secondary antibodies (Thermo Fisher Scientific) for 30 min, followed by 3 washes in PBTA and a wash in H_2O. Prolong Gold antifade reagent with 4′,6-diamidino-2-phenylindole (DAPI; Thermo Fisher Scientific) was used to mount slips on glass slides. Images were acquired on either a Leica DM55000 B upright microscope, a Zeiss Axio Imager upright microscope, or a Zeiss LSM510 confocal microscope.

FACS. U2OS GFP-LC3 cells were reverse transfected with 10 pmol of siRNA. Sixteen hours prior to fluorescence-activated cell sorting (FACS) analysis, cells were treated with either vehicle or 50 μM Cq. Seventy-two hours posttransfection, cells were trypsinized, washed twice with PBS, and fixed with ethanol (EtOH) for 30 min at 4°C. Cells were then washed twice with PBS and sorted by green fluorescent protein (GFP) fluorescence with a Beckman Coulter CyAn ADP using Summit 4.3 and analyzed with ModFit 4.0 DNA analysis software. A minimum of 1.0×10^4 events was used for analysis.

shSIK2 xenograft injections. A total of 8×10^5 SUM159 cells stably expressing pLKO.1 shSIK2 or a nontargeting control hairpin (200 μl) were injected in the right flank of NOD.cg-PRKDC^{SCID}Il2rg^{tm1Wjl}/SzJ (NSG) female mice, aged 4 to 6 weeks. Tumors were measured twice weekly using a digital caliper, and volume (V) was calculated using the following equation: V = (length of the longest side) × (length of the side perpendicular to the longest side)^2/(π/6). According to IACUC guidelines, mice bearing tumors greater than 2,000 mm^3 or exhibiting significantly diminished health were sacrificed. Tumors were surgically removed, weighed, and formalin fixed for 48 h. All studies were conducted in accordance with a UTSW IACUC-approved protocol.

RESULTS

To identify targetable vulnerabilities in TNBC, we implemented a tiered siRNA screening strategy to enrich for concordant responses among diverse oncogenomic backgrounds found in cell models of this disease. Given that the majority of TNBC tumors are classified as either claudin-low or basal-like subtype, we used cell lines representing both of these subtypes to account for biased vulnerabilities (7–9, 11). In the first tier of the analysis, we performed a genome-wide siRNA toxicity screen in the SUM159 claudin-low cell line (Fig. 1A and B; see also Table S1 in the supplemental material). As paclitaxel is a first-line chemotherapeutic in TNBC, we performed a 2-condition screen to assess consequences of gene depletion alone and in the presence of an innocuous dose (1 nM) of this agent (Fig. 1C). Here, we identified 30 candidate targets whose viability ratio (paclitaxel treated/untreated) was ≥5 standard deviations below the means (Fig. 1D). These 30 siRNAs were then evaluated for their activity in the WHIM12 (claudin-low), HCC1806 (basal-like), and SUM149 (basal-like) cell lines in the presence and absence of paclitaxel (Fig. 1E). This strategy identified SUM159-idiosyncratic siRNAs (NCOA6, LGR8, and MYO3A) as well as siRNAs with broad penetrance under all conditions tested (RBBP9, GLB1L2, KERA, and NNAT). We focused on siRNAs exhibiting selectivity within the panel, reasoning that these would be the least likely to target housekeeping functions in both tumor and normal cells. Among these, we identified salt-inducible kinase 2 (SIK2), whose depletion led to a dramatic loss in viability of SUM159 cells, moderate defects in WHIM12 and HCC1806, and no effect on SUM149 cells. This phenotype was observed with 2 independent siRNAs, both of which led to a strong reduction of SIK2 mRNA and protein levels (Fig. 1F). Knowledge of SIK2's contribution to tumorigenesis is limited to only two reports, which suggest an oncogenic function of this kinase in ovarian and prostate cancers (22, 23). Importantly, small-molecule SIK2 inhibitors are under active development to treat a number of human diseases, making this an actionable target in the near future (17, 31). Given the relative dearth of information on this therapeutically tractable protein, we focused follow-up efforts on its function in TNBC.

We further assessed the specificity of the SIK2 dependency in a panel of TNBC cell lines composed of 8 claudin-low, 8 basal-like, and 2 normal-immortalized cell lines (Fig. 2A). Here, 6 of the 8 claudin-low cell lines exhibited a loss of viability following siSIK2 transfection with 2 independent siRNAs. In contrast, only 1 of the 8 basal-like cell lines, HCC1806, appeared sensitive. Notably, this basal-like outlier is the only cell line derived from a primary acantholytic squamous cell carcinoma, a pathology distinct from that of ductal carcinomas. We observed minimal defects in the normal setting, indicating that the dependency on SIK2 was unique to the tumorigenic state. The viability decrease in the siSIK2-sensitive lines was not complete, as 30 to 40% of the population remained. Thus, we replated SIK2-depleted cells at limiting dilution to assess growth capacity of the residual population. Here, we observed a dramatic reduction in colony formation, suggesting that the majority of remaining cells were not viable following siSIK2 transfection (Fig. 2B). Furthermore, SIK2-depleted cells exhibited attenuated anchorage-independent growth, suggesting that SIK2 is required for tumorigenicity in TNBC (Fig. 2C).

We next evaluated the consequences of pharmacological inhibition of SIK2 on viability in TNBC. ARN-3236 is a recently developed ATP competitive inhibitor of SIK that associates with the hinge region. *In vitro*, ARN-3236 exhibits a 50% inhibitory concentration (IC_{50}) of 1 nM toward SIK2 (21.63 and 6.63 nM for SIK1 and SIK3, respectively) (17). To credential the effects of ARN-3236 on intact TNBC cells, we assayed its effects on phosphorylation of the well-characterized SIK2 substrate TORC2 (CRTC2) (12, 13, 25). Exposure of SUM159 cells to ARN-3236 for 6 h led to a reduction in phosphorylation of CRTC2, indicating inhibition of the SIK2 kinase (Fig. 2D) (12, 13). We treated a panel of TNBC cell lines with ARN-3236 and observed a decrease of >50% viability in two of the siSIK2-sensitive cell lines but limited defects in the siSIK2-resistant cell lines (Fig. 2E). The viability defect was also observed with a structurally distinct pan-SIK inhibitor, HG-9-91-01 (Fig. 2E) (31). Exposure of SUM159 cells to ARN-3236 also attenuated growth in soft agar, phenocopying the defect observed with siSIK2 (Fig. 2C and F). Taken together, these findings suggest that SIK2 is essential for viability and tumorige-

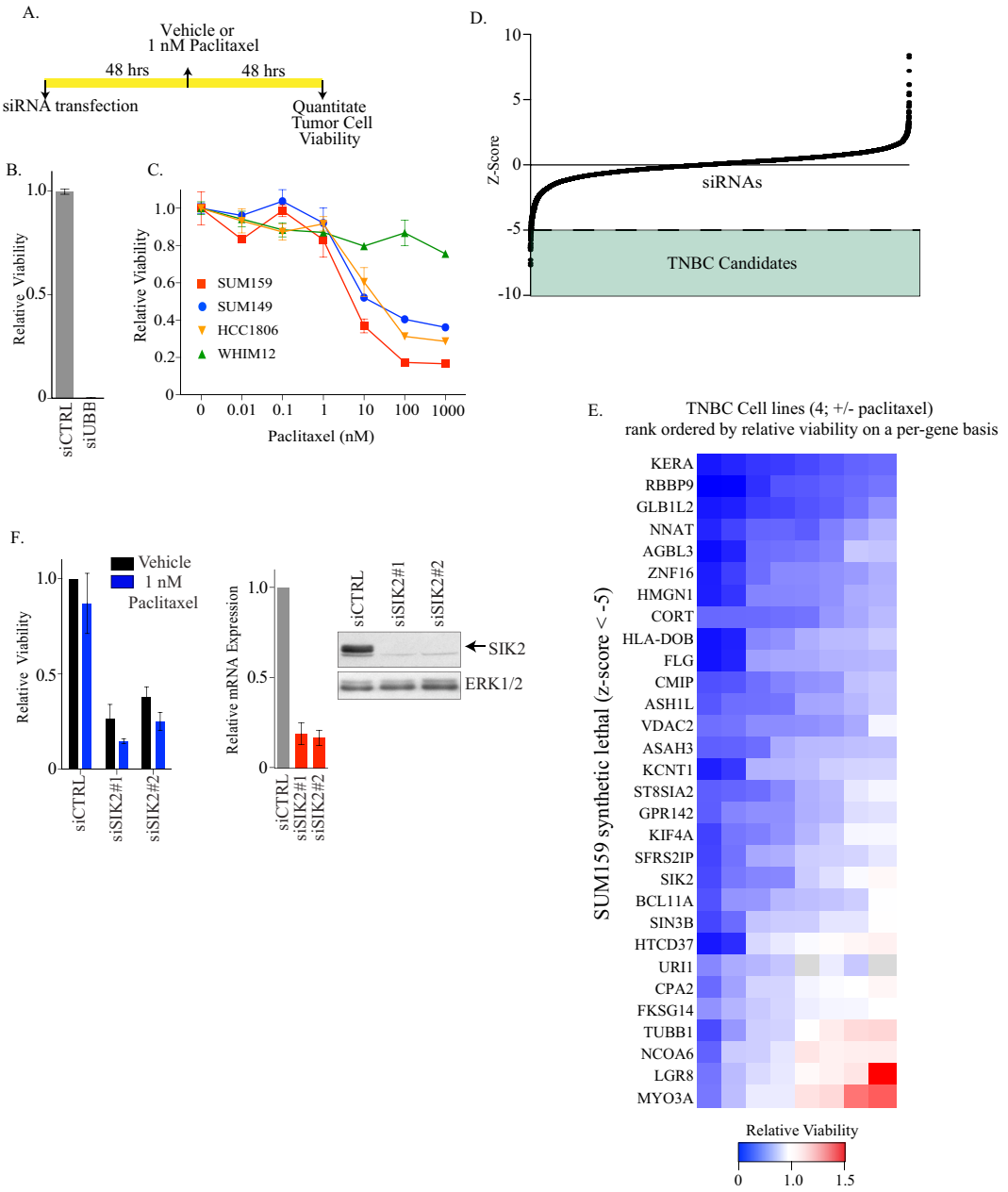

FIG 1 Pangenomic loss-of-function screen identified SIK2 as essential for TNBC. (A) Schematic for pangenomic siRNA screen. (B) SUM159 cells were transfected with control or ubiquitin B (UBB) siRNA for 96 h. Bars represent relative viability measured by CTG and range ($n = 2$). (C) Indicated cell lines were exposed to escalating doses of paclitaxel for 48 h. Points indicate viability as measured by CTG ($n = 2$; bars indicate the ranges). (D) Z-scores for each siRNA, ranked lowest to highest. siRNAs with Z-scores less than −5 are highlighted. (E) Heat map of viability scores (see Table S1 in the supplemental material) of 30 siRNAs identified in panel D in SUM159, SUM149, HCC1806, and WHIM12 with or without paclitaxel ranked by cell line penetrance. Gray coloring indicates unavailable values. (F, left) SUM159 cells were transfected with two independent SIK2 siRNAs. At 120 h posttransfection, cell viability was assessed by CTG. Bars represent average viability ($n \geq 5$; ±standard deviations [SD]). (Middle) As described for the left, except mRNA was collected at 72 h and SIK2 transcript measured by qPCR. Bars represent average values and ranges ($n = 2$). (Right) Whole-cell lysates (WCLs) from SUM159 transfected with the indicated siRNAs for 72 h were immunoblotted with the indicated antibodies.

nicity, particularly in the claudin-low subtype of TNBC, and pharmacological inhibition of this kinase is sufficient to reduce tumor growth.

A number of recent reports have implicated SIK2 in the modulation of autophagy (18, 21). Also, the expression of the tumor suppressor beclin-1 is lost in a subset of TNBC, suggesting that autophagy is altered in a subset of TNBC tumors (30). Thus, we examined the consequences of SIK2 depletion on accumulation of microtubule-associated protein light chain 3 (LC3), which associates with the autophagosomal membrane and can be used to monitor autophagic activity. Depletion of SIK2 led to a pronounced decrease in both LC3-I and -II accumulation in tumor and normal cell lines, irrespective of the effect of SIK2 on viability (Fig. 3A). Similarly, accumulation of p62, an adaptor protein found on au-

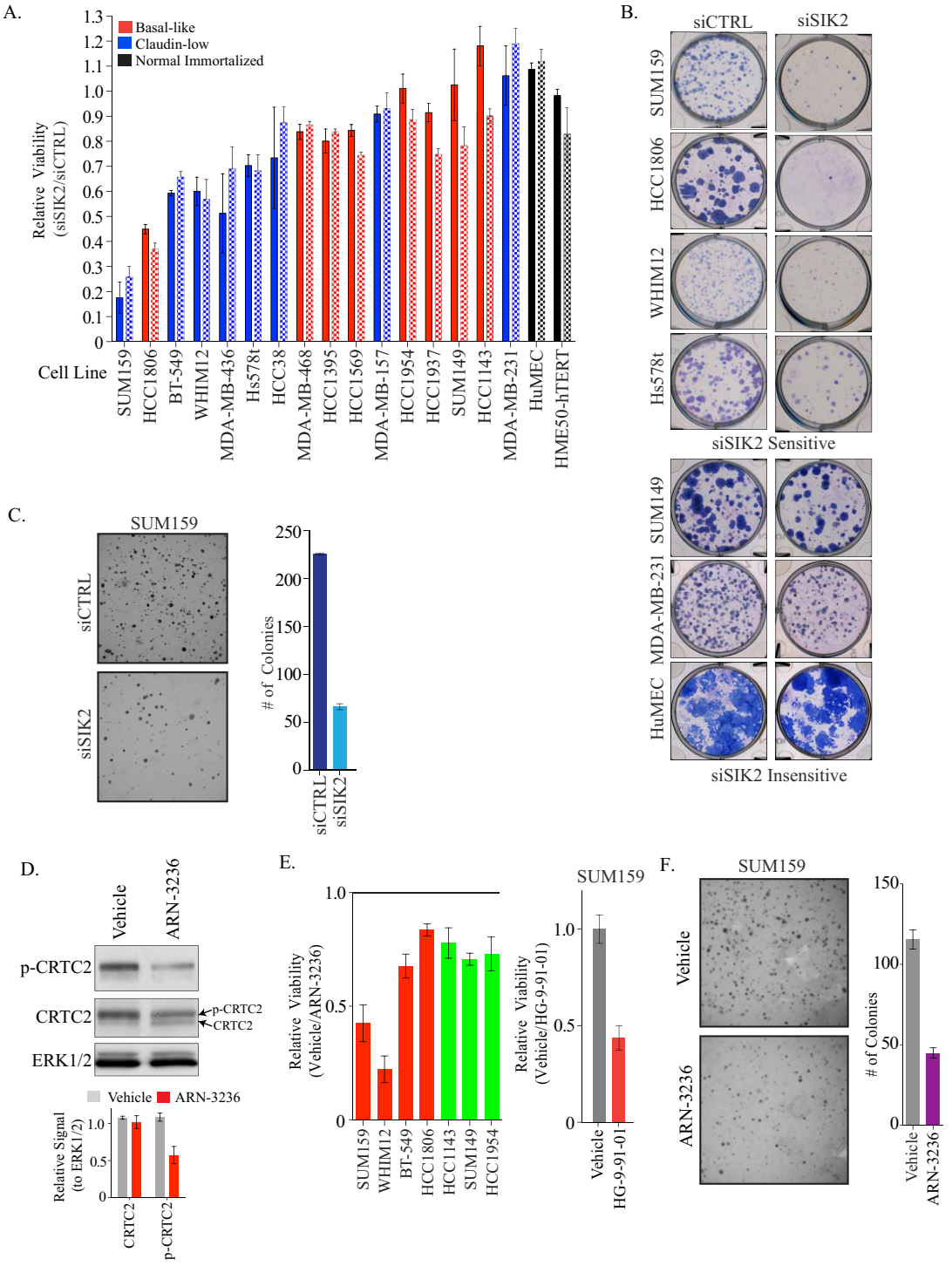

FIG 2 SIK2 is essential for viability in a subset of TNBC. (A) Indicated cell lines were transfected with siCTRL or siSIK2 for 120 h. Bars represent relative viability ($n = 3$; error bars indicate SD) measured by CTG. Solid bars are siRNA pool 1 and bars with hatch marks are pool 2. (B) Indicated cell lines were transfected with siCTRL or siSIK2 for 96 h and then replated at limiting dilution. (C) SUM159 cells were transfected for 24 h and then plated into soft agar. (Left) Images of stained colonies at 2 weeks after plating. (Right) Bars represent average colony numbers and ranges quantitated manually ($n = 2$). (D) SUM159 cells were exposed to 1 μM vehicle or ARN-3236 for 6 h. (Top) Whole-cell lysates were immunoblotted for the indicated antibodies. (Bottom) Quantitation of band intensity for each antibody relative to ERK1/2 over 2 independent experiments. (E) Indicated cells were plated in 96-well format and treated with the indicated compounds. Bars represent relative viability as determined by CTG assay ($n = 8$; ±SD). As defined for panel A, red bars indicate siSIK2 sensitive and green bars indicate siSIK2 resistant. (F) SUM159 cells were plated into soft agar and treated each day for 9 days with 1 μM ARN-3236. (Left) Representative images of stained colonies. (Right) Average number of colonies per condition quantitated manually ($n = 4$; ±SD).

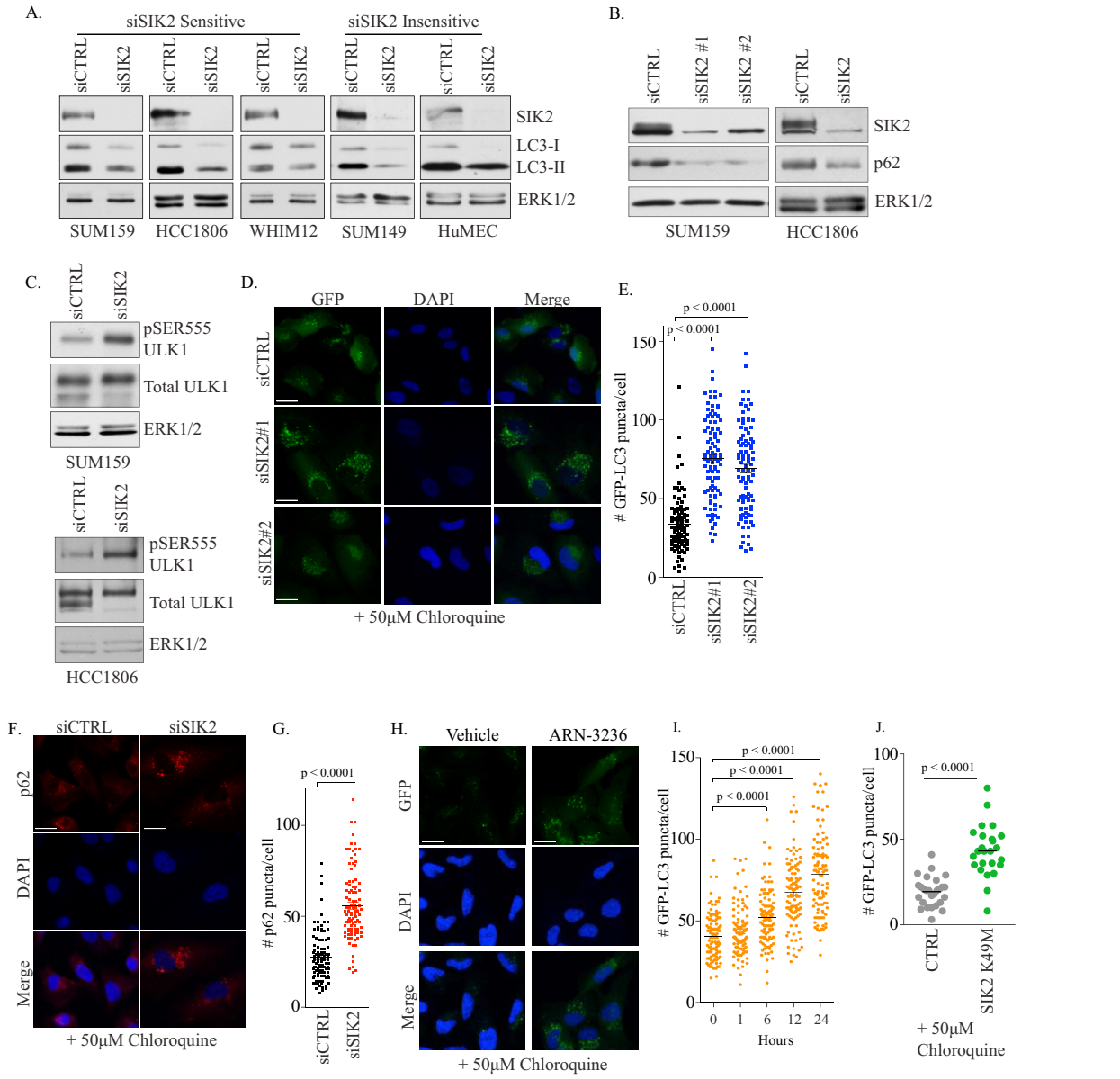

FIG 3 SIK2 restrict autophagy. (A to C) Immunoblots of WCLs from cells transfected with the indicated siRNAs for 72 h. (D) Representative confocal sections of SUM159-GFP-LC3 cells transfected with the indicated siRNAs for 72 h and exposed to 50 μM Cq for 4 h. Cells were fixed and stained with DAPI. Scale bars, 20 μm. (E) Cells treated as described for panel D were manually quantitated for GFP-positive puncta on an upright epifluorescence microscope. One hundred cells were quantitated per condition over two independent experiments. *P* values were calculated by Mann-Whitney test. (F) Representative confocal sections of SUM159 cells treated as described for panel D and stained with anti-p62 antibody and DAPI. Scale bars, 20 μm. (G) SUM159 cells treated as described for panel F were manually quantitated for p62-positive puncta on an upright epifluorescence microscope. One hundred cells were quantitated per condition over two independent experiments. *P* values were calculated by Mann-Whitney test. (H) SUM159-GFP-LC3 cells were exposed to 50 μM Cq for 9 h plus 1 μM ARN-3236 for 24 h. Representative confocal sections are presented. Scale bars, 20 μm. (I) GFP-LC3 puncta was quantitated in cells treated as described for panel H and treated with ARN-3236 for the indicated times. *P* values were calculated by Mann-Whitney test. (J) U2OS-GFP-LC3 stably expressing control (CTRL) or SIK2(K49M) cDNA were exposed to 50 μM Cq for 4 h. GFP-LC3 puncta in 25 transfected cells were manually quantitated using images acquired by confocal microscopy. *P* values were calculated using the two-tailed Mann-Whitney test.

tophagic vesicles, was also decreased in SIK2-depleted cells (Fig. 3B). The reduction of LC3 and p62 is consistent with enhanced vesicle flux through the pathway. To further evaluate this possibility, we assayed the activation of ULK1, which is phosphorylated on Ser555 by AMPK kinase as an initial step in autophagosome formation (32–34). Depletion of SIK2 led to a robust increase in phosphorylation on Ser555, indicating that autophagy was activated (Fig. 3C). We then stably expressed GFP-LC3 in SUM159 cells (SUM159-GFP-LC3) to monitor the accumulation of autophagic vesicles in single cells. We exposed cells to chloroquine (Cq), a lysosomotropic agent that leads to vesicle accumulation by preventing autophagosomal maturation. Under these conditions, SIK2 depletion led to a significant increase in the accumulation of GFP-LC3-positive vesicles (Fig. 3D and E). FACS analysis in

U20S-GFP-LC3 cells revealed that depletion of SIK2 enhanced GFP-LC3 accumulation, which was increased further upon Cq exposure (see Fig. S1A in the supplemental material). Notably, U20S cells also exhibited a reduction in viability upon depletion of SIK2 (see Fig. S1B). We also used p62 to monitor endogenous autophagosomes and found that SIK2 depletion and exposure to Cq led to an enhanced accumulation of p62-positive puncta (Fig. 3F and G).

To assess whether pharmacological inhibition of SIK2 phenocopied the siRNA phenotype, we exposed SUM159-GFP-LC3 cells to ARN-3236 in the presence of Cq. Here, we observed a time-dependent accumulation of GFP-LC3 vesicles, similar to the siRNA phenotype (Fig. 3H and I). We next asked whether the kinase activity was required for the observed changes in flux by stably overexpressing a kinase-dead mutant of SIK2 (K49M). Upon exposure to Cq, we observed an increase in autophagic flux, indicating that the kinase-dead mutant functions in a dominant-negative fashion (Fig. 3J). These data indicate that SIK2 restrains autophagy in TNBC, which in a specific subset of tumors is essential for survival.

We next evaluated whether the activation of autophagy upon SIK2 loss was responsible for the reduction in tumor cell viability. To do this, we performed an epistasis experiment in which autophagic vesicle formation was inhibited by depletion of ATG5, a key lipidation protein essential for the first steps in vesicle formation. In SUM159 cells, loss of ATG5 alone reduced GFP-LC3 vesicle accumulation and enhanced LC3-I, which is not associated with autophagosomes (Fig. 4A). Importantly, when SIK2 and ATG5 were codepleted, the ATG5 phenotype dominated, as we observed minimal vesicle formation and a stabilization of LC3-I (Fig. 4A and B). Moreover, codepletion of ATG5 rescued the loss of viability observed upon depletion of SIK2 alone (Fig. 4C and D). These data indicate that inhibition of SIK2 leads to excessive autophagy, which in certain TNBC settings results in cell death.

Findings thus far suggest that SIK2 is essential for viability, and its inhibition could be an antitumor strategy. Thus, we next assessed whether inhibition of SIK2 *in vivo* would reduce tumor growth (30). To test this possibility, we used shRNA to reduce SIK2 mRNA and protein in SUM159 cells (Fig. 4E). These cells were attenuated in their capacity to form colonies in soft-agar assays, mimicking the phenotypes observed with siSIK2 and ARN-3236 (Fig. 4F). Immediately following knockdown, these cells were implanted into the flanks of NSG mice and tumor growth was monitored for 6 weeks. Tumor initiation in shSIK2 tumors was significantly decreased and shSIK2 tumors were much smaller than those in the control group (Fig. 4G), suggesting that SIK2 is essential for tumorigenesis *in vivo*. Collectively, these results suggest that SIK2 functions in breast tumor and normal cells to restrain autophagic flux. In a subset of TNBC this function is essential for survival, and releasing this brake leads to cell death.

DISCUSSION

Treatment options in TNBC are limited to chemotherapy, radiation, and surgery. The response of individual patients to these intervention strategies is often unpredictable, incomplete, and ephemeral. There is an urgent need to identify new therapeutic entry points with associated predictive biomarkers to improve long-term outcomes for this patient population. The molecular classification of tumors into intrinsic subtypes presents an opportunity to determine if selective vulnerabilities exist among the different phenotypes within TNBC. By capitalizing on the faithful recapitulation of tumor subtypes in patient-derived cell lines, we find that SIK2 is selectively essential for survival particularly in the claudin-low subtype. Notably, this is the first identification of a molecular vulnerability aligned with the claudin-low disease, which is less sensitive to first-line chemotherapeutic regimens than other TNBC subtypes (7). Our findings may represent an important first step in tailoring treatment to this group of patients. In particular, ARN-3230 is an emerging SIK2 inhibitor for use in ovarian cancer patients that could be applied to the claudin-low setting. It is important to note that the alignment of SIK2 sensitivity was not uniform among the claudin-low cell lines tested. Additional investigations into molecular biomarkers that predict SIK2 sensitivity will be essential for more precisely identifying responsive patients.

Our findings suggest that SIK2 restricts autophagic flux. Autophagy has been implicated in both pro- and antitumorigenic function. For example, autophagy can be essential for tumor cell survival by limiting death due to hypoxia, inflammation, and chemotherapy (35–38). Conversely, suppression of autophagy has been unequivocally shown to limit tumorigenesis in mouse models (39–41). The contribution of autophagy to tumorigenesis is likely dependent on many factors, including the disease site and stage. Our findings suggest that autophagy is a tumor suppressor mechanism in claudin-low breast cancer. This result is also supported by human clinical studies demonstrating that beclin-1, an essential autophagy gene, is frequently lost in TNBC and correlates with poor survival (30). Our studies, particularly with ATG codepletion, suggest that the inhibition of SIK2 leads to an autophagic cell death (42). Whether autophagy itself is directly executing the cell death is unclear. It is possible that the unrestrained autophagy is leading to autolysis in sensitive cells (43). Perhaps the endoplasmic reticulum in SIK2-dependent cells is more easily depleted, leading to a rapid loss of viability once high levels of autophagy are activated. Alternatively, autophagy may be triggering cell death processes, such as necrosis or apoptosis, and SIK2 is required to prevent these mechanisms. Finally, activation of autophagy could kill only certain sets of tumor cells through the selective degradation of limiting substrates, including proteins or organelles such as mitochondria. Perhaps inhibition of autophagy is essential for maintenance of the mesenchymal and primordial features of claudin-low tumors, without which these tumor cells activate cell death programs. Reactivation of tumor suppressor functions lost during transformation is a particularly difficult therapeutic strategy. As we find that SIK2 may restrain autophagy, reinstating this antitumor function could be a feasible strategy through small-molecule inhibition of SIK2.

SIK2 has been implicated in promoting gluconeogenesis in liver and mitotic fidelity in ovarian and prostate cancers. In our system, we found no evidence that SIK2 inhibition led to mitotic defects (see Fig. S2 in the supplemental material). Furthermore, inhibition of CRTCs had no impact on the SIK2 phenotype in TNBC (not shown). Thus, our work, along with two prior reports, presents a strong case that SIK2 represents a novel autophagic regulatory pathway (18, 21). The molecular mechanisms that activate SIK2 and its downstream substrates are poorly described outside of gluconeogenesis. A recent exhaustive study in hepatocytes reported numerous putative phosphorylation events on SIK2 following fasting/glucagon exposure; however, none of these events led to a detectable alteration in intrinsic catalytic activity

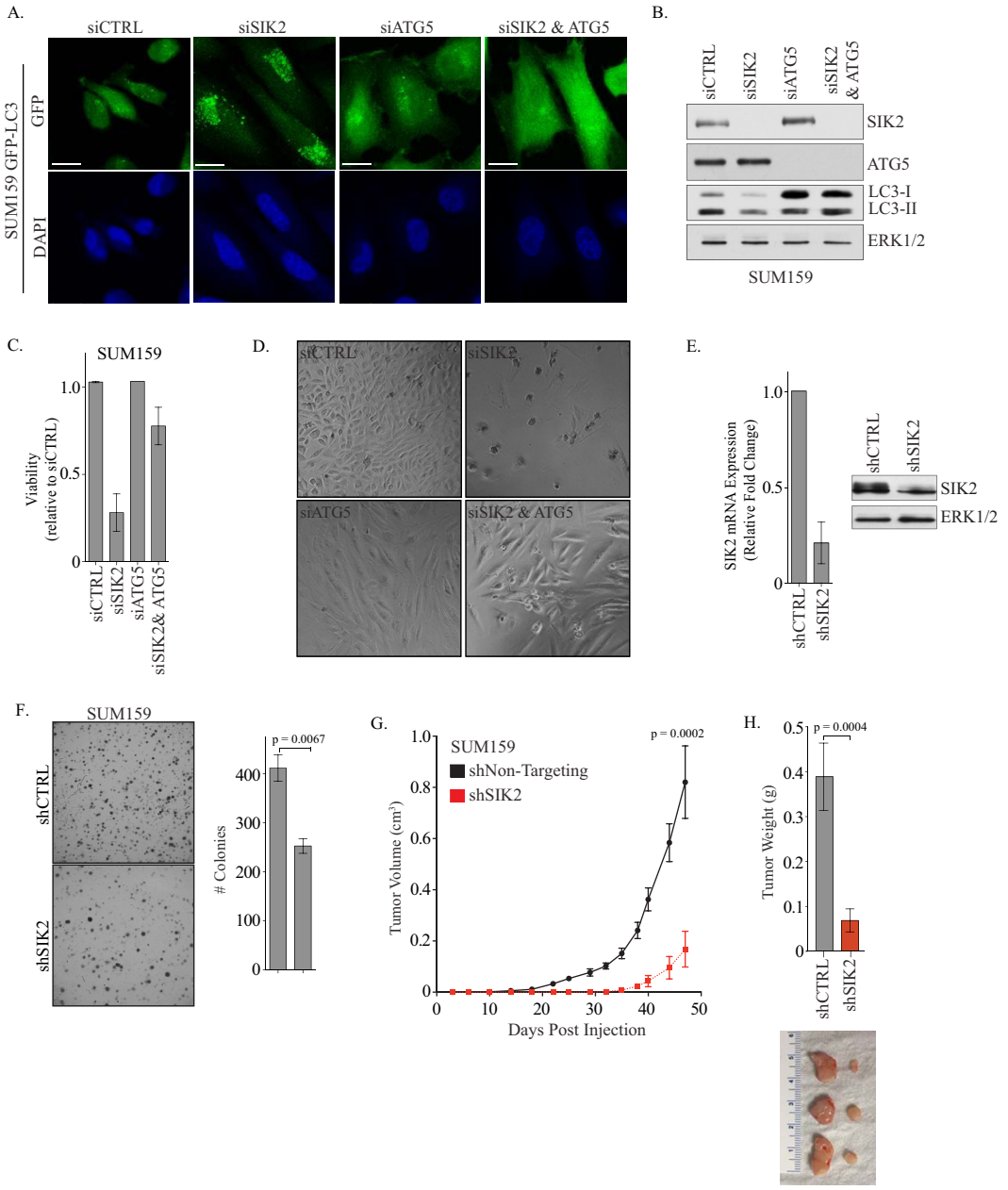

FIG 4 SIK2 restricts autophagy to support TNBC viability. (A) SUM159-GFP-LC3 cells were transfected with the indicated siRNAs for 72 h and exposed to 50 μM Cq for 16 h. Cells were fixed, stained with DAPI, and visualized for GFP. Representative images were captured by epifluorescence. Scale bars, 20 μm. (B) Cells were transfected with the indicated siRNAs for 72 h. WCLs were immunoblotted with the indicated antibodies. (C) Cell lines were transfected with the indicated siRNAs for 96 h (SUM159). Bars represent average relative viability and ranges ($n = 2$) measured by CTG. (D) Bright-field images of SUM159 cells transfected as described for panel C. (E) SUM159 cells were infected with lentivirus encoding shCTRL or shSIK2 hairpins for 2 days. (Left) Relative SIK2 mRNA expression was measured by qPCR in SUM159 cells stably expressing the indicated shRNAs. Bars represent average levels of SIK2 mRNA and range ($n = 2$). (Right) WCLs from cells shown on the left were immunoblotted for the indicated antibodies. (F) Cells shown in panel E were plated into soft agar. Bars represent the average number of colonies quantitated manually ($n = 3 \pm$ standard errors of the means [SEM]). The *P* value was calculated using a two-tailed Student *t* test. (G) Growth curves of SUM159 cells shown in panel E were injected subcutaneously in NSG mice, and tumor volume was measured at the indicated time points. Points represent average volumes of shCTRL ($n = 10$) or shSIK2 ($n = 10$) ± SEM. The *P* value was calculated with an unpaired, two-tailed Student *t* test. (H) At the study endpoint, tumors were excised and weighed. (Top) Bars represent mean tumor weights ± SEM. The *P* value was calculated with an unpaired, two-tailed Student *t* test and are indicated on the graph. (Bottom) Images of tumors expressing the indicated shRNAs.

(31). Low-stearic-hindrance gatekeeper residues, such as SIKs, are associated with higher basal kinase activity (27). Thus, it is possible that SIK2 activity undergoes negative regulation by upstream kinases, as has been shown for PKA. Furthermore, the only well-validated SIK substrates are CRTC1-3 and HDAC4 (12, 13, 44). One report suggested that SIK2 resides on autophagic vesicles, presenting the possibility that it directly phosphorylates key regulators of vesicle formation. Taken together, our findings present a

fresh phenotypic context to study SIK2 regulatory processes that impinge on autophagy in both the normal and transformed states.

ACKNOWLEDGMENTS

We thank Brian Golitz for assistance with siRNA screens, Brandt Nichols for assistance with animal experiments, and Aleix Prat and Charles Perou for breast cancer cell lines.

Hariprasad Vankayalapati is chief scientific officer and founder of Arrien Pharmaceuticals.

FUNDING INFORMATION

K.E.M. was supported by general medicine training grant T32GM007040-37. A.W.W. is supported by NIH grant CA154699. The Simmons Cancer Center Support Grant 5P30 CA142543-05 supported shared resources used in this study at UTSW. This work was also supported by CA058223.

REFERENCES

1. **Hammond ME, Hayes DF, Dowsett M, Allred DC, Hagerty KL, Badve S, Fitzgibbons PL, Francis G, Goldstein NS, Hayes M, Hicks DG, Lester S, Love R, Mangu PB, McShane L, Miller K, Osborne CK, Paik S, Perlmutter J, Rhodes A, Sasano H, Schwartz JN, Sweep FC, Taube S, Torlakovic EE, Valenstein P, Viale G, Visscher D, Wheeler T, Williams RB, Wittliff JL, Wolff AC.** 2010. American Society of Clinical Oncology/College Of American Pathologists guideline recommendations for immunohistochemical testing of estrogen and progesterone receptors in breast cancer. J Clin Oncol **28:**2784–2795. http://dx.doi.org/10.1200/JCO.2009.25.6529.
2. **Jahanzeb M.** 2008. Adjuvant trastuzumab therapy for HER2-positive breast cancer. Clin Breast Cancer **8:**324–333. http://dx.doi.org/10.3816/CBC.2008.n.037.
3. **Slamon DJ, Leyland-Jones B, Shak S, Fuchs H, Paton V, Bajamonde A, Fleming T, Eiermann W, Wolter J, Pegram M, Baselga J, Norton L.** 2001. Use of chemotherapy plus a monoclonal antibody against HER2 for metastatic breast cancer that overexpresses HER2. N Engl J Med **344:**783–792. http://dx.doi.org/10.1056/NEJM200103153441101.
4. **Prat A, Lluch A, Albanell J, Barry WT, Fan C, Chacon JI, Parker JS, Calvo L, Plazaola A, Arcusa A, Segui-Palmer MA, Burgues O, Ribelles N, Rodriguez-Lescure A, Guerrero A, Ruiz-Borrego M, Munarriz B, Lopez JA, Adamo B, Cheang MC, Li Y, Hu Z, Gulley ML, Vidal MJ, Pitcher BN, Liu MC, Citron ML, Ellis MJ, Mardis E, Vickery T, Hudis CA, Winer EP, Carey LA, Caballero R, Carrasco E, Martin M, Perou CM, Alba E.** 2014. Predicting response and survival in chemotherapy-treated triple-negative breast cancer. Br J Cancer **111:**1532–1541. http://dx.doi.org/10.1038/bjc.2014.444.
5. **Onitilo AA, Engel JM, Greenlee RT, Mukesh BN.** 2009. Breast cancer subtypes based on ER/PR and Her2 expression: comparison of clinicopathologic features and survival. Clin Med Res **7:**4–13. http://dx.doi.org/10.3121/cmr.2008.825.
6. **Perou CM, Sorlie T, Eisen MB, van de Rijn M, Jeffrey SS, Rees CA, Pollack JR, Ross DT, Johnsen H, Akslen LA, Fluge O, Pergamenschikov A, Williams C, Zhu SX, Lonning PE, Borresen-Dale AL, Brown PO, Botstein D.** 2000. Molecular portraits of human breast tumours. Nature **406:**747–752. http://dx.doi.org/10.1038/35021093.
7. **Prat A, Parker JS, Karginova O, Fan C, Livasy C, Herschkowitz JI, He X, Perou CM.** 2010. Phenotypic and molecular characterization of the claudin-low intrinsic subtype of breast cancer. Breast Cancer Res **12:**R68. http://dx.doi.org/10.1186/bcr2635.
8. **Lehmann BD, Bauer JA, Chen X, Sanders ME, Chakravarthy AB, Shyr Y, Pietenpol JA.** 2011. Identification of human triple-negative breast cancer subtypes and preclinical models for selection of targeted therapies. J Clin Investig **121:**2750–2767. http://dx.doi.org/10.1172/JCI45014.
9. **Neve RM, Chin K, Fridlyand J, Yeh J, Baehner FL, Fevr T, Clark L, Bayani N, Coppe JP, Tong F, Speed T, Spellman PT, DeVries S, Lapuk A, Wang NJ, Kuo WL, Stilwell JL, Pinkel D, Albertson DG, Waldman FM, McCormick F, Dickson RB, Johnson MD, Lippman M, Ethier S, Gazdar A, Gray JW.** 2006. A collection of breast cancer cell lines for the study of functionally distinct cancer subtypes. Cancer Cell **10:**515–527. http://dx.doi.org/10.1016/j.ccr.2006.10.008.
10. **Sorlie T, Perou CM, Tibshirani R, Aas T, Geisler S, Johnsen H, Hastie T, Eisen MB, van de Rijn M, Jeffrey SS, Thorsen T, Quist H, Matese JC, Brown PO, Botstein D, Lonning PE, Borresen-Dale AL.** 2001. Gene expression patterns of breast carcinomas distinguish tumor subclasses with clinical implications. Proc Natl Acad Sci U S A **98:**10869–10874. http://dx.doi.org/10.1073/pnas.191367098.
11. **Prat A, Karginova O, Parker JS, Fan C, He X, Bixby L, Harrell JC, Roman E, Adamo B, Troester M, Perou CM.** 2013. Characterization of cell lines derived from breast cancers and normal mammary tissues for the study of the intrinsic molecular subtypes. Breast Cancer Res Treat **142:**237–255. http://dx.doi.org/10.1007/s10549-013-2743-3.
12. **Dentin R, Liu Y, Koo SH, Hedrick S, Vargas T, Heredia J, Yates J, III, Montminy M.** 2007. Insulin modulates gluconeogenesis by inhibition of the coactivator TORC2. Nature **449:**366–369. http://dx.doi.org/10.1038/nature06128.
13. **Screaton RA, Conkright MD, Katoh Y, Best JL, Canettieri G, Jeffries S, Guzman E, Niessen S, Yates JR, III, Takemori H, Okamoto M, Montminy M.** 2004. The CREB coactivator TORC2 functions as a calcium- and cAMP-sensitive coincidence detector. Cell **119:**61–74. http://dx.doi.org/10.1016/j.cell.2004.09.015.
14. **Itoh Y, Sanosaka M, Fuchino H, Yahara Y, Kumagai A, Takemoto D, Kagawa M, Doi J, Ohta M, Tsumaki N, Kawahara N, Takemori H.** 2015. Salt-inducible kinase 3 signaling is important for the gluconeogenic programs in mouse hepatocytes. J Biol Chem **290:**17879–17893. http://dx.doi.org/10.1074/jbc.M115.640821.
15. **Nixon M, Stewart-Fitzgibbon R, Fu J, Akhmedov D, Rajendran K, Mendoza-Rodriguez MG, Rivera-Molina YA, Gibson M, Berglund ED, Justice NJ, Berdeaux R.** 2016. Skeletal muscle salt inducible kinase 1 promotes insulin resistance in obesity. Mol Metab **5:**34–46. http://dx.doi.org/10.1016/j.molmet.2015.10.004.
16. **Park J, Yoon YS, Han HS, Kim YH, Ogawa Y, Park KG, Lee CH, Kim ST, Koo SH.** 2014. SIK2 is critical in the regulation of lipid homeostasis and adipogenesis in vivo. Diabetes **63:**3659–3673. http://dx.doi.org/10.2337/db13-1423.
17. **Lombardi MS, Gillieron C, Dietrich D, Gabay C.** 2016. SIK inhibition in human myeloid cells modulates TLR and IL-1R signaling and induces an anti-inflammatory phenotype. J Leukoc Biol **99:**711–721. http://dx.doi.org/10.1189/jlb.2A0715-307R.
18. **Potts MB, Kim HS, Fisher KW, Hu Y, Carrasco YP, Bulut GB, Ou YH, Herrera-Herrera ML, Cubillos F, Mendiratta S, Xiao G, Hofree M, Ideker T, Xie Y, Huang LJ, Lewis RE, MacMillan JB, White MA.** 2013. Using functional signature ontology (FUSION) to identify mechanisms of action for natural products. Sci Signal **6:**ra90.
19. **Sanosaka M, Fujimoto M, Ohkawara T, Nagatake T, Itoh Y, Kagawa M, Kumagai A, Fuchino H, Kunisawa J, Naka T, Takemori H.** 2015. Salt-inducible kinase 3 deficiency exacerbates lipopolysaccharide-induced endotoxin shock accompanied by increased levels of pro-inflammatory molecules in mice. Immunology **145:**268–278. http://dx.doi.org/10.1111/imm.12445.
20. **Sundberg TB, Choi HG, Song JH, Russell CN, Hussain MM, Graham DB, Khor B, Gagnon J, O'Connell DJ, Narayan K, Dancik V, Perez JR, Reinecker HC, Gray NS, Schreiber SL, Xavier RJ, Shamji AF.** 2014. Small-molecule screening identifies inhibition of salt-inducible kinases as a therapeutic strategy to enhance immunoregulatory functions of dendritic cells. Proc Natl Acad Sci U S A **111:**12468–12473. http://dx.doi.org/10.1073/pnas.1412308111.
21. **Yang FC, Tan BC, Chen WH, Lin YH, Huang JY, Chang HY, Sun HY, Hsu PH, Liou GG, Shen J, Chang CJ, Han CC, Tsai MD, Lee SC.** 2013. Reversible acetylation regulates salt-inducible kinase (SIK2) and its function in autophagy. J Biol Chem **288:**6227–6237. http://dx.doi.org/10.1074/jbc.M112.431239.
22. **Ahmed AA, Lu Z, Jennings NB, Etemadmoghadam D, Capalbo L, Jacamo RO, Barbosa-Morais N, Le XF, Australian Ovarian Cancer Study Group, Vivas-Mejia P, Lopez-Berestein G, Grandjean G, Bartholomeusz G, Liao W, Andreeff M, Bowtell D, Glover DM, Sood AK, Bast RC, Jr.** 2010. SIK2 is a centrosome kinase required for bipolar mitotic spindle formation that provides a potential target for therapy in ovarian cancer. Cancer Cell **18:**109–121. http://dx.doi.org/10.1016/j.ccr.2010.06.018.
23. **Bon H, Wadhwa K, Schreiner A, Osborne M, Carroll T, Ramos-Montoya A, Ross-Adams H, Visser M, Hoffmann R, Ahmed AA, Neal DE, Mills IG.** 2014. Salt-inducible kinase 2 regulates mitotic progression and transcription in prostate cancer. Mol Cancer Res **13:**620–635. http://dx.doi.org/10.1158/1541-7786.MCR-13-0182-T.
24. **Cheng H, Liu P, Wang ZC, Zou L, Santiago S, Garbitt V, Gjoerup OV,**

Iglehart JD, Miron A, Richardson AL, Hahn WC, Zhao JJ. 2009. SIK1 couples LKB1 to p53-dependent anoikis and suppresses metastasis. Sci Signal **2:**ra35.

25. **Clark K, MacKenzie KF, Petkevicius K, Kristariyanto Y, Zhang J, Choi HG, Peggie M, Plater L, Pedrioli PG, McIver E, Gray NS, Arthur JS, Cohen P.** 2012. Phosphorylation of CRTC3 by the salt-inducible kinases controls the interconversion of classically activated and regulatory macrophages. Proc Natl Acad Sci U S A **109:**16986–16991. http://dx.doi.org/10.1073/pnas.1215450109.
26. **Bain J, Plater L, Elliott M, Shpiro N, Hastie CJ, McLauchlan H, Klevernic I, Arthur JS, Alessi DR, Cohen P.** 2007. The selectivity of protein kinase inhibitors: a further update. Biochem J **408:**297–315. http://dx.doi.org/10.1042/BJ20070797.
27. **Gum RJ, McLaughlin MM, Kumar S, Wang Z, Bower MJ, Lee JC, Adams JL, Livi GP, Goldsmith EJ, Young PR.** 1998. Acquisition of sensitivity of stress-activated protein kinases to the p38 inhibitor, SB 203580, by alteration of one or more amino acids within the ATP binding pocket. J Biol Chem **273:**15605–15610. http://dx.doi.org/10.1074/jbc.273.25.15605.
28. **Wang Z, Canagarajah BJ, Boehm JC, Kassisa S, Cobb MH, Young PR, Abdel-Meguid S, Adams JL, Goldsmith EJ.** 1998. Structural basis of inhibitor selectivity in MAP kinases. Structure **6:**1117–1128. http://dx.doi.org/10.1016/S0969-2126(98)00113-0.
29. **White E.** 2015. The role for autophagy in cancer. J Clin Investig **125:**42–46. http://dx.doi.org/10.1172/JCI73941.
30. **Tang H, Sebti S, Titone R, Zhou Y, Isidoro C, Ross TS, Hibshoosh H, Xiao G, Packer M, Xie Y, Levine B.** 2015. Decreased mRNA expression in human breast cancer is associated with estrogen receptor-negative subtypes and poor prognosis. EBioMedicine **2:**255–263. http://dx.doi.org/10.1016/j.ebiom.2015.01.008.
31. **Patel K, Foretz M, Marion A, Campbell DG, Gourlay R, Boudaba N, Tournier E, Titchenell P, Peggie M, Deak M, Wan M, Kaestner KH, Goransson O, Viollet B, Gray NS, Birnbaum MJ, Sutherland C, Sakamoto K.** 2014. The LKB1-salt-inducible kinase pathway functions as a key gluconeogenic suppressor in the liver. Nat Commun **5:**4535.
32. **Kim J, Kundu M, Viollet B, Guan KL.** 2011. AMPK and mTOR regulate autophagy through direct phosphorylation of Ulk1. Nat Cell Biol **13:**132–141. http://dx.doi.org/10.1038/ncb2152.
33. **Hara T, Takamura A, Kishi C, Iemura S, Natsume T, Guan JL, Mizushima N.** 2008. FIP200, a ULK-interacting protein, is required for autophagosome formation in mammalian cells. J Cell Biol **181:**497–510. http://dx.doi.org/10.1083/jcb.200712064.
34. **Egan DF, Chun MG, Vamos M, Zou H, Rong J, Miller CJ, Lou HJ, Raveendra-Panickar D, Yang CC, Sheffler DJ, Teriete P, Asara JM, Turk BE, Cosford ND, Shaw RJ.** 2015. Small molecule inhibition of the autophagy kinase ULK1 and identification of ULK1 substrates. Mol Cell **59:**285–297. http://dx.doi.org/10.1016/j.molcel.2015.05.031.
35. **Degenhardt K, Mathew R, Beaudoin B, Bray K, Anderson D, Chen G, Mukherjee C, Shi Y, Gelinas C, Fan Y, Nelson DA, Jin S, White E.** 2006. Autophagy promotes tumor cell survival and restricts necrosis, inflammation, and tumorigenesis. Cancer Cell **10:**51–64. http://dx.doi.org/10.1016/j.ccr.2006.06.001.
36. **Guo JY, Chen HY, Mathew R, Fan J, Strohecker AM, Karsli-Uzunbas G, Kamphorst JJ, Chen G, Lemons JM, Karantza V, Coller HA, Dipaola RS, Gelinas C, Rabinowitz JD, White E.** 2011. Activated Ras requires autophagy to maintain oxidative metabolism and tumorigenesis. Genes Dev **25:**460–470. http://dx.doi.org/10.1101/gad.2016311.
37. **Lock R, Kenific CM, Leidal AM, Salas E, Debnath J.** 2014. Autophagy-dependent production of secreted factors facilitates oncogenic RAS-driven invasion. Cancer Discov **4:**466–479. http://dx.doi.org/10.1158/2159-8290.CD-13-0841.
38. **Hu YL, Jahangiri A, Delay M, Aghi MK.** 2012. Tumor cell autophagy as an adaptive response mediating resistance to treatments such as antiangiogenic therapy. Cancer Res **72:**4294–4299. http://dx.doi.org/10.1158/0008-5472.CAN-12-1076.
39. **Liang XH, Jackson S, Seaman M, Brown K, Kempkes B, Hibshoosh H, Levine B.** 1999. Induction of autophagy and inhibition of tumorigenesis by beclin 1. Nature **402:**672–676. http://dx.doi.org/10.1038/45257.
40. **Wei H, Wei S, Gan B, Peng X, Zou W, Guan JL.** 2011. Suppression of autophagy by FIP200 deletion inhibits mammary tumorigenesis. Genes Dev **25:**1510–1527. http://dx.doi.org/10.1101/gad.2051011.
41. **Mathew R, Karp CM, Beaudoin B, Vuong N, Chen G, Chen HY, Bray K, Reddy A, Bhanot G, Gelinas C, Dipaola RS, Karantza-Wadsworth V, White E.** 2009. Autophagy suppresses tumorigenesis through elimination of p62. Cell **137:**1062–1075. http://dx.doi.org/10.1016/j.cell.2009.03.048.
42. **Galluzzi L, Vitale I, Abrams JM, Alnemri ES, Baehrecke EH, Blagosklonny MV, Dawson TM, Dawson VL, El-Deiry WS, Fulda S, Gottlieb E, Green DR, Hengartner MO, Kepp O, Knight RA, Kumar S, Lipton SA, Lu X, Madeo F, Malorni W, Mehlen P, Nunez G, Peter ME, Piacentini M, Rubinsztein DC, Shi Y, Simon HU, Vandenabeele P, White E, Yuan J, Zhivotovsky B, Melino G, Kroemer G.** 2012. Molecular definitions of cell death subroutines: recommendations of the Nomenclature Committee on Cell Death 2012. Cell Death Differ **19:**107–120. http://dx.doi.org/10.1038/cdd.2011.96.
43. **Liu Y, Shoji-Kawata S, Sumpter RM, Jr, Wei Y, Ginet V, Zhang L, Posner B, Tran KA, Green DR, Xavier RJ, Shaw SY, Clarke PG, Puyal J, Levine B.** 2013. Autosis is a Na+,K+-ATPase-regulated form of cell death triggered by autophagy-inducing peptides, starvation, and hypoxia-ischemia. Proc Natl Acad Sci U S A **110:**20364–20371. http://dx.doi.org/10.1073/pnas.1319661110.
44. **Henriksson E, Sall J, Gormand A, Wasserstrom S, Morrice NA, Fritzen AM, Foretz M, Campbell DG, Sakamoto K, Ekelund M, Degerman E, Stenkula KG, Goransson O.** 2015. SIK2 regulates CRTCs, HDAC4 and glucose uptake in adipocytes. J Cell Sci **128:**472–486. http://dx.doi.org/10.1242/jcs.153932.